Symmetric periodic Anderson model in infinite dimensions

M. Jarrell
Institute for Theoretical Physics, University of California, Santa Barbara, California 93106
and Department of Physics, University of Cincinnati, Cincinnati, Ohio 45221-0011
(Received 29 July 1994)

The symmetric periodic Anderson model is studied in the limit of infinite spatial dimensions with an essentially exact quantum Monte Carlo method. As the temperature is lowered $T < T_0$, the properties of the system cross over from those of a metal with a moderately heavy mass, to those of an insulator in which the one- and two-particle spectra develop gaps $\approx T_0$, where T_0 is the Wilson Kondo scale. Whereas the quasiparticle gap $\approx T_0$ is indirect in momentum, the optical conductivity displays a much larger direct gap. T_0 is much larger in the symmetric lattice than in the impurity problem with the same parameters. Depending upon the ratio of T_0 to the Ruderman-Kittel-Kasuya-Yosida exchange energy, there is a transition to an antiferromagnetic state. In the paramagnetic state, the f-electron linear specific heat shows scaling with T/T_0, whereas the f-electron contribution to the bulk susceptibility shows only a rough scaling with T/T_0 with deviations that are consistent with the strength of the net ferromagnetic exchange.

I. INTRODUCTION AND METHOD

Since the discovery of the heavy-fermion materials with rare-earth or actinide elements[1] the periodic Anderson model (PAM) was considered as the most promising candidate to at least qualitatively describe the rich physics in these materials. From early studies it is known that most of the unusual properties of these materials like the large coefficient in the specific heat, transport properties, and even magnetic and superconducting properties can be qualitatively accounted for with the PAM.[1] Quantitative agreement with experiments is sometimes possible due to the fact that over a large region these systems may be regarded as a regular array of *independent* Kondo scatterers, which makes it possible to calculate especially thermodynamic[1,2] and even transport[3] quantities using the well-understood impurity Anderson model.

However, in view of the controversial two-particle properties of these materials it is desirable to have an exact solution of the *periodic* Anderson model in a nontrivial limit. A quite general limit to obtain sensible approximate or even exact results for such *locally* highly correlated models is the limit of infinite dimensions.[4–6] In this limit the dynamics of the system become essentially local,[5] which considerably simplifies the task of calculating physical quantities.[6] Recently, several groups independently proposed a mean-field theory for the Hubbard model based on the special properties in this limit[7–10] and were able to calculate a variety of quantities approximately[9] or even essentially exactly.[10,11] In this paper, we apply this procedure to the periodic Anderson model. In combination with exact quantum Monte Carlo (QMC) procedures,[12] we calculate one- and two-particle properties of this model which can be viewed as essentially *exact* results for the periodic Anderson model in a nontrivial limit.

Although the inclusion of more realistic features presents no fundamental difficulty for our method, we want to concentrate on the simplest version of the periodic Anderson model in D dimensions,

$$H=\frac{-t^*}{2\sqrt{D}}\sum_{\langle ij\rangle\sigma} d^\dagger_{i\sigma}d_{j\sigma}+\text{H.c.}+\sum_{i\sigma}(\epsilon_d d^\dagger_{i\sigma}d_{i\sigma}+\epsilon_f f^\dagger_{i\sigma}f_{i\sigma}) +\sum_i U(n_{fi\uparrow}-1/2)(n_{fi\downarrow}-1/2) +V\sum_{i\sigma}(d^\dagger_{i\sigma}f_{i\sigma}+\text{H.c.})\,. \tag{1}$$

In (1), $d\,(f)^{(\dagger)}_{i\sigma}$ destroys (creates) a $d\,(f)$ electron on site i with spin σ, U is the screened Coulomb-matrix element for the localized f states, and V characterizes the mixing between the two subsystems.

Although the lattice structure is not essential to our arguments, we will study the model (1) on a simple hypercubic lattice of dimension D with hybridization $t=t^*/2\sqrt{D}$ restricted to near-neighbor hopping. This surely is an oversimplifying assumption for real systems; however, it has the advantage that the free density of states in the limit $D\rightarrow\infty$ becomes purely Gaussian, $N^{d0}(\epsilon)=\exp\{-(\epsilon/t^*)^2\}/\sqrt{\pi t^{*2}}$, with a width t^*. We choose $t^*=1$ as a convenient energy scale for the remainder of this paper.

Since dynamics become essentially local for $D=\infty$,[4,5] one can use the fact that the proper one-particle self-energy is then **k** independent to resume the perturbation series and obtain an effective impurity Anderson model with a self-consistently determined medium.[7–10] For the Hamiltonian (1), these equations read

$$G^f_{ii,\sigma}(z)=\int d\epsilon\rho^{(0)}_d(\epsilon)\{z-\epsilon_f-\Sigma_\sigma(z) +V^2[z-\epsilon_d-\epsilon]^{-1}\}^{-1}\,, \tag{2}$$

$$\mathcal{G}(z)=[(G^f_{ii,\sigma}(z))^{-1}+\Sigma_\sigma(z)]^{-1}\,, \tag{3}$$

where $G^f_{ij,\sigma}(z)$ denotes the one-particle Green's function for the f states and $\mathcal{G}(z)$ is the noninteracting (U turned

off) local Green's function with the effect of integrating out all the other f sites included. The self-energy in Eq. (3) comes from allowing U to act. $\mathcal{G}(z)$ is to be used as the initial Green's function in a QMC procedure,[10] or as the bare Green's function in a perturbative expansion for the local self-energy.[13] Equations (2) and (3) form a closed system which determines $\Sigma(z)$. The difficulty remains that, in order to obtain a refined $\Sigma(z)$ from an initial guess, one has to solve the impurity Anderson model defined by (3). Among the several different approaches to this problem, quantum Monte Carlo (QMC) (Ref. 12) is the most efficient for the current purposes, since it (i) is essentially exact in that the errors are small and controllable and (ii) allows us to address two-particle properties in addition to the real-frequency spectra.[10] A detailed discussion of the application of QMC to lattice systems in the infinite-dimensional limit has appeared elsewhere.[14] In this paper we will regard QMC only as a source for the one- and two-particle Green's function measured on the impurity site.

These local Green's function provide sufficient information to calculate all of the thermodynamics and equilibrium transport quantities in the infinite-dimensional limit. For example, the one-particle f and d (and fd) Green's function may be constructed from $\Sigma(i\omega_n)$ obtained from solving Eqs. (2) and (3),

$$G^d(\mathbf{k},i\omega_n)=\frac{1}{i\omega_n-\epsilon_d-\epsilon_{\mathbf{k}}-V^2/[i\omega_n-\epsilon_f-\Sigma(i\omega_n)]}\ , \tag{4}$$

$$G^f(\mathbf{k},i\omega_n)=\frac{1}{i\omega_n-\epsilon_f-\Sigma(i\omega_n)-V^2/(i\omega_n-\epsilon_d-\epsilon\mathbf{k})}\ . \tag{5}$$

As described in Appendix A, with the additional knowledge of the two-particle one-site Greens' function, one may calculate the corresponding lattice susceptibility for any $x(\mathbf{q})$, where $x(\mathbf{q})=(1/d)\sum_l \cos(q_l)$ defines an equivalence class of wave vectors in the infinite-dimensional Brillouin zone.[5] In this way, the magnetic, charge, and superconducting lattice susceptibilities are calculated.

It is also possible to calculate the real-frequency dynamics of the model by analytically continuing the on-site Green's function. For example, if the on-site f Green's function $G^f(\mathbf{R}=\mathbf{0},\omega)$ is calculated by numerical analytic continuation,[15] the real-frequency self-energy may then be obtained by inverting the Fadeev function $w(z)$ (Ref. 16) in

$$G^f(\mathbf{R}=\mathbf{0},\omega)=[1+i\sqrt{\pi}w(\gamma(\omega))V^2/\alpha(\omega)]/\alpha(\omega)\ , \tag{6}$$

where $\gamma=\omega-\epsilon_d-V^2/\alpha$ and $\alpha=\omega-\epsilon_f-\Sigma(\omega)$. Since the current-current susceptibility is free of vertex corrections in the infinite-dimensional limit[17] and since, in the absence of a momentum-dependent fd hybridization V, the current operator may be written exclusively in terms of the d-electron operators,[18] knowledge of $\Sigma(\omega)$ is sufficient to calculate the optical conductivity. In fact, the form of the equations for the optical conductivity is identical to those for the Hubbard model,[10] when both are written as functions of the local conduction-band Green's function $G^d(\mathbf{R}=\mathbf{0},\omega)$ and γ.

II. RESULTS

Recently, there has been renewed interest in a special class of cubic lanthanide-based compounds such as CeNiSn (Ref. 19) or $Ce_3Bi_4Pt_3$ (Refs. 20 and 21) which show a behavior reminiscent of normal heavy-fermion materials at high temperatures but become insulating at low temperatures where they develop both transport and spin gaps. In these materials the f-electron contribution to experimental measurements is isolated by taking the difference of measurements on the Ce compound and the isostructural La analog.[19–21] The symmetric periodic Anderson model, $\epsilon_f=\epsilon_d=0$, is used to model these materials since it also displays heavy-fermion-like properties at high temperatures, and develops a (pseudo) gap in the one-particle excitation spectrum at low temperatures.[22,23] It is, therefore, interesting to study its relevance for these materials.

A. Hybridization gap

The essential physical feature in the symmetric model is the formation of a gap in the various spectra. As shown in Fig. 1(a), this gap forms quite rapidly in the single-particle density of states as the temperature is lowered. Since the chemical potential is at the center of the gap ($\omega=0$), an insulator forms at low temperature. The occurrence of this insulating state is directly connected to the perfect particle-hole symmetry in the present case and has a rather intuitive physical reason: As $T<T_0$ where T_0 is the Kondo temperature which will be discussed in Sec. II B, the Kondo effect leads to a scattering resonance at the chemical potential. In fact, as shown in Fig. 1(b), where the f-electron contribution to the density of states is isolated, one can see that a broad Kondo resonance begins to form when $T\gtrsim T_0$ before the gap opens. Since there exists a level crossing between these dynamically generated local quasiparticle states and

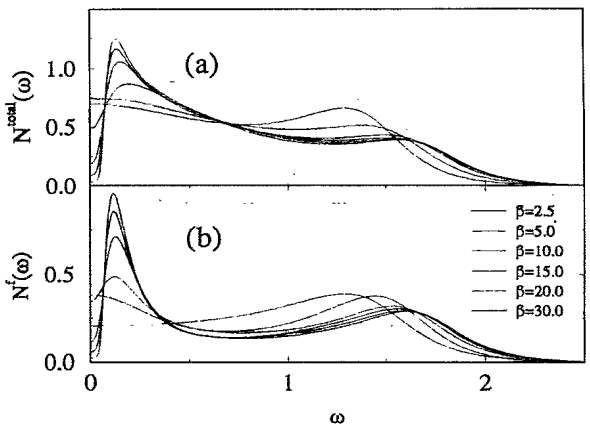

FIG. 1. Temperature dependence of the total density of states (a) $N_{\rm tot}(\omega)$ and the f-electron density of states (b) $N_f(\omega)$ when $V=0.5$, $U=2.0$, $\epsilon_f=\epsilon_d=0$, and $T_0=0.23$.

the conduction-band states, as the temperature is lowered further one will find a splitting with a gap at the position of the resonance.[24] For the particle-hole symmetry under consideration the resonance develops exactly at the chemical potential,[22,23] i.e., the resulting system consequently is an insulator.

As shown in Fig. 2, the size of the gap in the density of states is roughly $\Delta \approx T_0/2$, when measured from zero frequency to the location of the maximum,[25] independent of the parameters chosen. Thus, many of the thermodynamic and transport properties of the system should show some sort of scaling with T/T_0. There is also a spin gap in the local f-electron dynamic susceptibility. To lowest order, the gap in the dynamic susceptibility results from particle-hole excitations across the insulating gap. Thus, the width of this gap, when measured from $\omega=0$ to the peak is about twice the quasiparticle gap $\Delta_s \approx 2\Delta$, when measured in the same way. A similar gap ratio, $\Delta_s/\Delta \approx 2$ is seen in the Anderson insulator $Ce_3Bi_4P_3$.[21]

Evidence for the gap may also be seen in the thermodynamics properties of the system like the bulk charge and spin susceptibilities. These are plotted as a function of temperature when $U=2$ and $V=0.6$ in Fig. 3. Consistent with what is seen in $Ce_3Bi_4Pt_3$,[20] the ferromagnetic susceptibility displays a broad peak when $T \approx T_0$. Note that both the charge and the spin susceptibilities share similar features, in that they both fall to essentially zero once the gap forms in the single-particle density states. Notice also that this occurs at the same temperature for both, indicating that for the infinite-dimensional PAM, the spin and charge gap have the same value, $\Delta_s=\Delta_c \approx 2\Delta$. This is in contrast to the one-dimensional Kondo lattice, where the charge gap is always larger than the spin gap, especially for the small value of $J_{fd} \sim 8V^2/U$ (Refs. 26 and 27) used in Fig. 3. Apparently

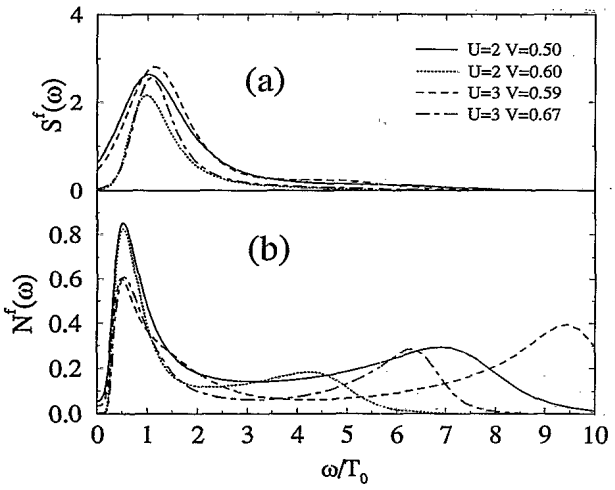

FIG. 2. Local neutron structure factor $S^f(\omega)$ (a), and f-electron single-particle density of states $N^f(\omega)$ (b) when $T=0.05$, and $\epsilon_f=\epsilon_d=0$ for various values of V and U. The rough coincidence of the gap in each figure indicates that the gap is proportional to T_0 (since the plots correspond to different values of T/T_0, one does not expect the plots to exactly coincide).

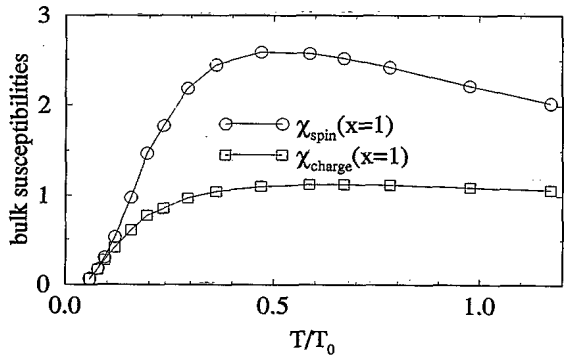

FIG. 3. Spin and charge susceptibilities for the symmetric PAM when $U=2$ and $V=0.6$. Both susceptibilities develop a gap of the same magnitude at low T.

the nonlocal charge and spin excitations found in finite dimensions, but not in $D=\infty$, are responsible for the larger value of Δ_c/Δ_s.

The optical conductivity, shown in Fig. 4, also displays a gap as $T/T_0 \to 0$. There is a Drude peak centered at $\omega=0$, which loses its spectral weight as $T/T_0 \to 0$ and the system becomes insulating. At higher frequencies, there is another peak which results from direct (momentum conserving) particle-hole excitations across the single-particle gap. Finally, there is a very small tail extending to $\omega \approx U=2$ associated with charge transfer on and off the f orbital. In the inset, the quasiparticle energies are plotted versus $\epsilon_k=-2t\sum_{l=1}^{D}\cos(k_l)$ when $\beta=30$, the smallest direct gap $E_{direct}/T_0 \approx 2.83$ occurs when $\epsilon_k=0$. The value of E_{direct}/T_0 is represented as an $*$ in the main plot. The energy of the low-temperature optical gap corresponds to the direct gap in the quasiparticle spectrum rather than $T_0/2$ (the indirect gap) due to the lack of nonlocal dynamical excitations (i.e., magnons, plasmons, or acoustic phonons) in the infinite-dimensional limit which would facilitate lower-energy indirect transitions.

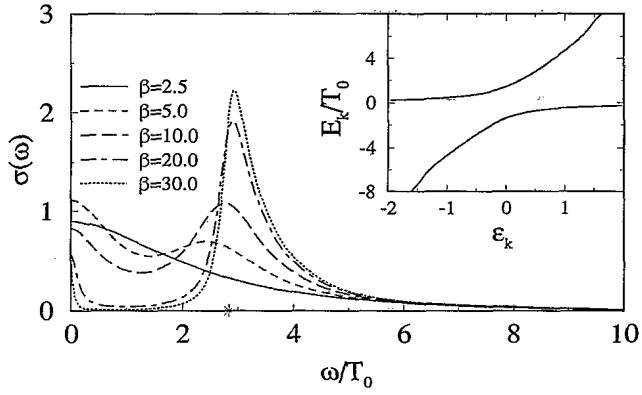

FIG. 4. Optical conductivity of the symmetric PAM when $U=2$, $V=0.5$, and $T_0=0.23$. The $*$ coincides with the minimum direct gap in the quasiparticle energy when $\beta=30$. The corresponding quasiparticle energy defined by $\mathrm{Re}\{1/G^d(E_k,\epsilon_k)\}=0$ is shown in the inset.

B. Kondo temperature

In the Anderson impurity problem it is possible to define a Kondo scale T_0 which is determined by the additional low-temperature susceptibility due to the introduction of the impurity into an otherwise pure host, $\chi_{\rm imp}(T=0)=1/T_0$. In order to define a similar energy scale in the lattice system, it is useful to think about the infinite-dimensional PAM as a self-consistently embedded impurity problem. Once convergence of the self-consistency has been obtained, it is possible to consider the simulated site as an impurity embedded in a host characterized by the d-electron propagator. Then, consistent with Wilson's definition of the Kondo scale,[28] we define $T_0=\lim_{t\to 0}1/\chi_{\rm imp}(T)$, where $\chi_{\rm imp}$ is the total additional susceptibility which results from the addition of the impurity to the host defined by the fully-dressed d-electron propagator. The calculation of $\chi_{\rm imp}$ is discussed in Appendix C. The limit $T\to 0$ can be approximated by extrapolation. This is shown in Fig. 5 where $1/T_0\chi(T)$ is plotted vs T/T_0 from several different data sets. The results from different sets can roughly be collapsed onto the same curve with an appropriate choice of T_0 for each dataset.[29] The corresponding values of T_0 are listed in the legend.

To gain some perspective on this result, it is useful to compare the PAM value of T_0 with the Anderson impurity model value. To do this, we simulated a single Anderson impurity embedded in an uncorrelated Gaussian d band with $N^d(\epsilon)=\exp\{-(\epsilon)^2\}/\sqrt{\pi}$ in the symmetric limit $\epsilon_d=\epsilon_f=0$. We measured the additional susceptibility due to the introduction of the impurity into an otherwise pure noninteracting host, $\chi_{\rm imp}$. The Kondo temperature T_K is then determined by comparing $\chi_{\rm imp}(T)$ to the universal Anderson impurity result of Krishna-murthy, Wilkins, and Wilson.[30] This result when multiplied by $(\pi/2)^2$ gives $T_0=(\pi/2)^2T_K$.[28,31] We calculated the impurity T_0 for each of the values of U and V discussed in Fig. 5. As tabulated in Table I, the impurity T_0 is significantly smaller than the lattice T_0. Our results are consistent with those of Rice and Ueda who employed a Gutzwiller approximation,[32] and found that the impurity

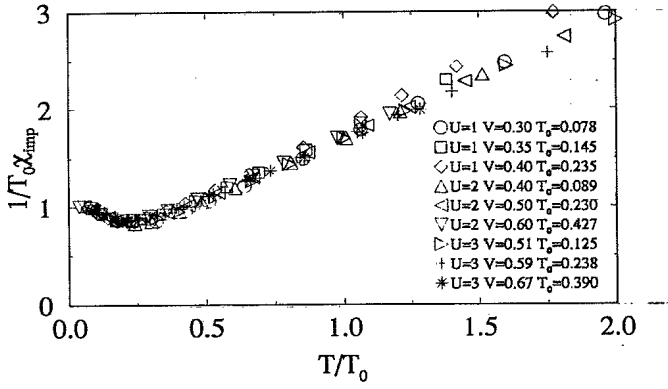

FIG. 5. $1/T_0\chi_{\rm imp}(T)$ vs T/T_0 for various data sets. T_0 was chosen so that $1/T_0\chi_{\rm imp}(0)=1$. When chosen in this way, the data collapse onto a single curve (Ref. 29), indicating universality of $\chi_{\rm imp}(T)$.

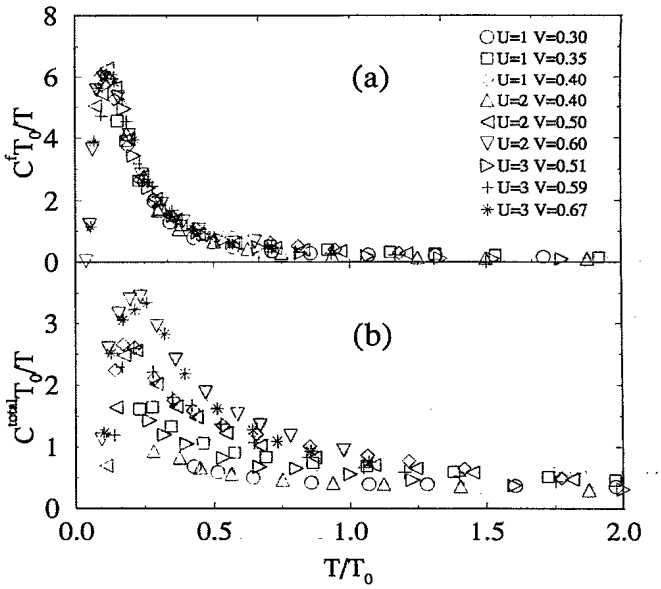

FIG. 6. The f electron (a) contribution to the linear specific heat, and the total lattice linear specific heat (b). The f-electron result shows scaling with T/T_0.

Kondo scale is $\exp(-1/2N^{d0}(0)J)$ smaller than the lattice T_0. A similar effect was seen in simulations of the one-dimensional Kondo lattice.[26] This demonstrates that the f moments significantly renormalize the properties of the conduction band, and that the symmetric lattice model is both significantly less correlated and has a significantly different temperature dependence than the Anderson impurity model.

If T_0 were the only small energy scale in the problem, then many of the f-electron properties of the system should show scaling with T/T_0. For example, the f-electron and total lattice specific heat are plotted versus T/T_0 in Fig. 6. The f-electron specific heat was calculated by measuring the f-electron contribution to the energy per site and evaluating the thermal derivative; whereas the total lattice specific heat is the derivative of the total energy per site. Clearly, the f-electron specific heat is relatively universal, whereas the total lattice specific heat is not.

C. Magnetic properties

Of course, T_0 is not the only small energy scale to be found in the PAM. The magnetic exchange energy will cause deviations from universality, especially for quantities which are sensitive to it. For example, in Fig. 7 the f electron and total lattice bulk magnetic susceptibilities are plotted. Again, the f-electron contribution is closer to universal than the total lattice susceptibility. However, there clearly are deviations from scaling which are well outside of the systematic and statistical errors involved in the QMC process. As shown in the inset, the deviations from scaling correlate with the strength of the net ferromagnetic exchange. This demonstrates the importance of the magnetic exchange.

Magnetic transitions in the PAM are determined by

TABLE I. Kondo scales for the symmetric impurity problem and the PAM. In each case, the impurity $T_{0\,\mathrm{imp}}$ is significantly less than the lattice $T_{0\,\mathrm{lattice}}$. The measured ratio of $T_{0\,\mathrm{imp}}/T_{0\,\mathrm{lattice}}$ is qualitatively consistent with the Gutzwiller result $\exp(-1/2N^{d0}(0)J)$[32] when J_{fd} is approximated as $J_{fd}=8V^2/U$.

U	V	$T_{0\,\mathrm{imp}}$	$T_{0\,\mathrm{lattice}}$	$T_{0\,\mathrm{imp}}/T_{0\,\mathrm{lattice}}$	$\exp(-1/2N^{d0}(0)J_{fd})$
1	0.30	0.0199	0.078	0.255	0.292
1	0.35	0.0483	0.145	0.333	0.405
1	0.40	0.0933	0.235	0.397	0.500
2	0.40	0.0197	0.089	0.221	0.250
2	0.50	0.0802	0.230	0.349	0.412
2	0.60	0.1957	0.427	0.458	0.540
3	0.51	0.0211	0.125	0.169	0.279
3	0.59	0.0594	0.238	0.250	0.384
3	0.67	0.1280	0.390	0.328	0.477

the competition between Kondo screening of the moments and this magnetic exchange. The former favors paramagnetism, while the latter favors antiferromagnetism in the symmetric model. In order to explore these two effects, we have calculated both the screened and unscreened moments of the system, as well as the Ruderman-Kittel-Kasuyer-Yosida (RKKY) magnetic exchange as described in Appendix B.

In Fig. 8, the screened $T\chi^f_{ii}(T)$ and unscreened $\langle(n_{f\sigma}-n_{f-\sigma})^2\rangle$ local f moments of the system are plotted vs T/T_0. As expected, the screened local moment is significantly reduced by the Kondo effect when $T<T_0$. However, it is also interesting to note that the unscreened moment is also reduced when $T\lesssim T_0$. This effect has also been seen in simulations of the one-dimensional Anderson lattice.[33,34] To interpret this effect, it is useful to consider the infinite-dimensional PAM as a self-consistently embedded Anderson impurity problem. For the impurity problem, $\langle(n_{f\sigma}-n_{f-\sigma})^2\rangle$ changes little with T/T_0, but may be reduced by either increasing the hybridization rate $\pi V^2N^{d0}(0)$, or decreasing U. To see which is happening here, consider the single-particle spectra shown in Fig. 1. Here, the high-energy peaks, associated with f-d charge transfer, shift significantly upward when the temperature is lowered, $T\lesssim T_0$. This is consistent with an increase in the impurity hybridization rate, since a reduction in U would cause these peaks to shift to lower frequencies. This reduction in the unscreened moment is consistent with the increase in the PAM value of T_0 when compared to the impurity result. Thus, a phenomenological explanation for the increase in T_0 for the symmetric lattice is that the opening of the hybridization gap corresponds to an increase in the hybridization rate of the impurity problem, leading to a reduction in the unscreened moments.

These moments interact through both RKKY and superexchange. For large U, the net magnetic exchange is dominated by the RKKY exchange, since the superexchange contribution falls off more quickly with increasing U. In Appendix B, the RKKY exchange is approximated with fourth-order perturbation theory in V. The resulting exchange always favors anitferromagnetism in the sym-

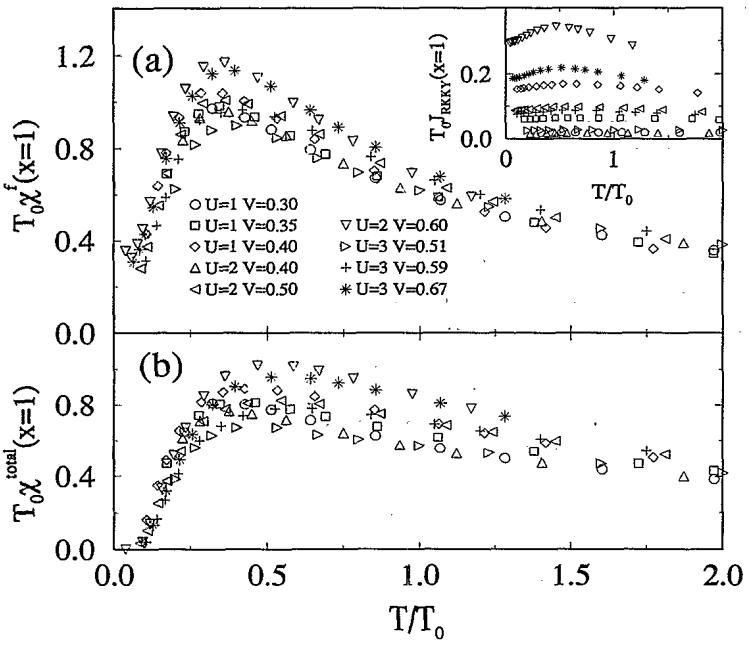

FIG. 7. The f-electron (a) and total lattice (b) bulk magnetic susceptibilities vs T/T_0. The f-electron contribution is closer to universal than the total lattice susceptibility; however, deviations from scaling are still apparent, indicating the importance of the exchange energy. In the inset, the net ferromagnetic RKKY exchange is plotted versus T/T_0. The deviations from scaling found in (a) correlate with the strength of $T_0J_{\mathrm{RKKY}}(x=1)$.

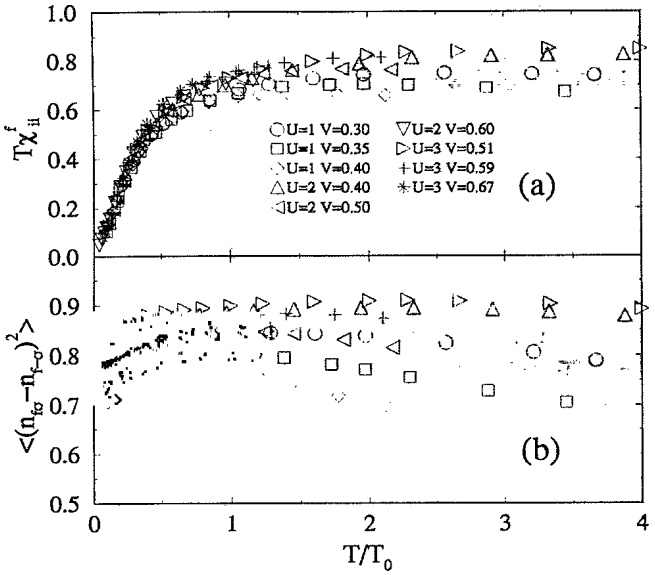

FIG. 8. The screened $T\chi^f_{ii}(T)$ and unscreened $\langle(n_{f\sigma}-n_{f-\sigma})^2\rangle$ local f moments vs T/T_0.

metric PAM; i.e., as shown in the inset to Fig. 9, $J_{\mathrm{RKKY}}(x(\mathbf{q}))$ is maximum at $x(\mathbf{q})=-1$. In order to compare the energy per site that the system can gain by forming a paramagnetic Kondo ground state $\sim T_0$ to that which can be gained by forming the Néel state $E_{\mathrm{RKKY}}[x(\mathbf{q})=-1]$ (which we approximate by the product of $J_{\mathrm{RKKY}}[x(\mathbf{q})=-1]$ and the square of the unscreened moment), we plot the ratio of these energies in Fig. 9. When $E_{\mathrm{RKKY}}/T_0 \gtrsim 1$, we expect that the system will undergo an antiferromagnetic transition as the temperature is lowered, and when $E_{\mathrm{RKKY}}/T_0 \lesssim 1$, we expect a paramagnetic ground state.

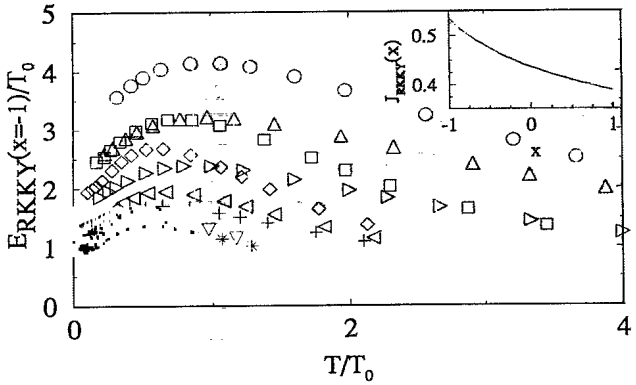

FIG. 9. The approximate ratio of the energy to be gained per site by forming an antiferromangetic state $E_{\mathrm{RKKY}}[x(\mathbf{q})=-1]$ (which we approximate by the product of $J_{\mathrm{RKKY}}[x(\mathbf{q})=-1]$ and the square of the unscreened moment), and the energy to be gained by forming a paramagnetic (Kondo screened) state T_0 (the symbols have the same meaning as those used in Fig. 8). When this ratio is large, one expects the system to display an antiferromagnetic transition. In the inset, the RKKY exchange is plotted vs $x(\mathbf{q})$ when $U=2$, $V=0.5$, and $\beta=20$. The largest exchange occurs at the zone corner $x(\mathbf{q})=-1$, indicating that an antiferromagnetic state is favored.

The transition is seen in Fig. 10, where the antiferromagnetic total lattice susceptibility is plotted versus T/T_0. In the infinite-dimensional limit,the susceptibilities display mean-field behavior, $1/\chi(x,T)\sim T-T_c(x)$. Thus, the transition temperatures may be determined by interpolating (or extrapolating) the inverse susceptibilities to zero as a function of T. This is shown in the inset to Fig. 10. As expected, the datasets which do not display a transition are those with the smallest values of $E_{\mathrm{RKKY}}(x(\mathbf{q})=-1)/T_0$. In each case displayed in Fig. 10 where a transition was found, $T_N<T_0$, so that Kondo screening and the hybridization gap always begin to form *before* the transition.

This competition between screening and exchange can also be seen in the phase diagram of the symmetric model. For example, T_N is plotted vs U for fixed $V=0.6$ in Fig. 11(a). For small U the screening dominates, and the ground state is a paramagnetic insulator (of course for $U\approx 0$, the system is a band insulator[35]), whereas for $U\gtrsim 2.5$ the system undergoes an antiferromagnetic transition. However, for $U\gtrsim 2.5$, T_N is still reduced by Kondo screening, since without Kondo screening, one expects that $T_N\approx E_{\mathrm{RKKY}}(x=-1)$. The screening reduces T_N so that $T_N<E_{\mathrm{RKKY}}(x=-1)$.

In addition, T_N falls quite slowly after the peak value is reached. If the magnetic exchange in the symmetric PAM is approximated with fourth-order perturbation theory in V using the *undressed* conduction-band propagators,[36,34] then the resulting RKKY interaction $J\sim J^2_{fd}\sim 1/U^2$ for large U. Thus, one expects that $T_N\sim 1/U^2$ in the strong coupling limit, i.e., when the unscreened moment saturates so that $J_{\mathrm{RKKY}}(x=-1)\approx E_{\mathrm{RKKY}}(x=-1)$. However, we find that T_N falls more slowly with increasing U, at least in the range of large to intermediate U [this same behavior was also seen in a recent slave-Boson calculation of the symmetric PAM (Ref. 37)]. There appear to be at least two reasons for this. First, the RKKY interaction, when constructed from *fully-dressed* conduction-band propagators obtained from the QMC, falls slowly with increasing U. This is due to the fact that the quasiparticle gap, which suppresses the particle-hole excitations which characterize the RKKY exchange, decreases as U increases. In fact, the antiferromagnetic RKKY exchange may roughly be fit to $J_{\mathrm{RKKY}}(x=-1)=a+b/U$, as shown by the solid line in Fig. 11(b). Second, the effects of screening are reduced when U increases, further favoring the formation of an antiferromagnetic state. This is because T_0 falls more quickly with increasing U than does $E_{\mathrm{RKKY}}(x=-1)$. In fact, as shown by the dashed line, the Wilson Kondo scale may be fit to an exponential form $T_0=c\exp(-bU)$, and the ratio $T_0/E_{\mathrm{RKKY}}(x=-1)$ appears to fall monotonically with increasing U, indicating that the Kondo screening declines more quickly than the net antiferromagnetic exchange.

D. Superconductivity

The superconducting properties of the heavy-fermion compounds are especially interesting and controversial.

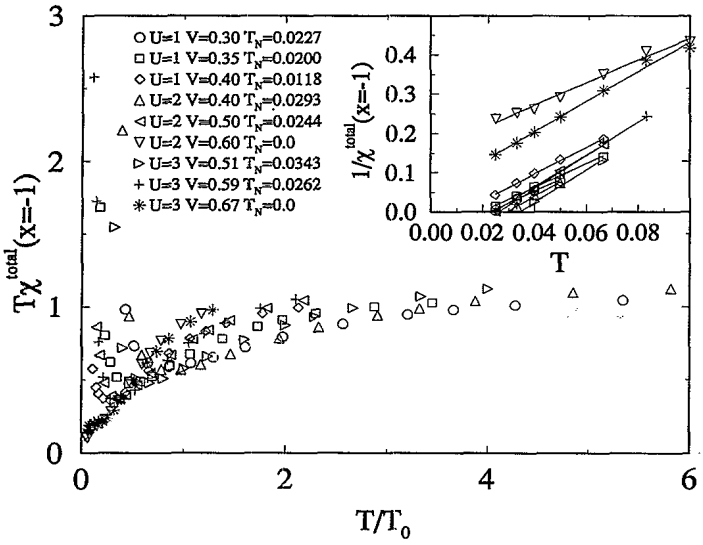

FIG. 10. The product of the lattice antiferromagnetic susceptibility and temperature versus T/T_0. In the inset, the inverse susceptibility is plotted vs T. The transition temperature may be determined by interpretation or extrapolation with the form $1/\chi^{\text{total}}(x,T) \sim T - T_c(x)$. Note that the datasets which do not display a transition are those with the smallest value of $E_{\text{RKKY}}[x(\mathbf{q}=-1)]/T_0$ shown in Fig. 9.

In the infinite-dimensional PAM, as in the infinite-dimensional Hubbard model, pairing with symmetries orthogonal to the lattice is not supported.[10] Thus, we need only look for s-wave pairing. Recently, Coleman, Miranda, and Tsvelik[38] explored the properties of the symmetric Kondo lattice model (which may be approximated with the PAM in the limit as $U \to \infty$) with a Mijorana-fermion mean-field theory. They found that the ground state of the symmetric model was an odd-frequency superconductor.[39] Thus, we will look for both odd- and even-frequency s-wave pairing.

To do this, we calculate the on-site s-wave pair-field susceptibility and use a frequency form factor to project out the odd and even parts as described in Appendix A. We found that both of these pair-field susceptibilities were always largest at the zone center $x(\mathbf{q})=1$, and that the odd-frequency susceptibility was always much larger than the even-frequency susceptibility, suggesting that the strong local correlations always suppressed the even-frequency pairing. The transition temperature may then be calculated by extrapolation of $1/P(x=1) \sim T - T_c$. As shown in Fig. 12, the extrapolated value of T_c is always negative, indicating that no transition was found. Indeed no transition was found for any of the datasets explored.

III. CONCLUSION

We have provided an essentially exact solution of the infinite-dimensional PAM. For brevity, we have concentrated on the symmetric model, and shown that the spectra, specific heat, and susceptibility are heavy-fermion-like for high T/T_0, and insulatorlike for low T/T_0. The f-electron linear specific heat shows scaling with T/T_0, whereas the f-electron contribution to the bulk susceptibility shows a rough scaling with T/T_0 with deviations which are consistent with the strength of the net ferromagnetic exchange. At low temperatures, the single-particle spectra shows a quasiparticle gap $\Delta \approx T_0/2$, whereas the gap in the dynamic spin susceptibility is twice this size $\Delta_s \approx T_0$. From the behavior of the charge and spin bulk susceptibilities, we infer that the charge and spin gaps are identical in the infinite-dimensional limit $\Delta_c = \Delta_s$.

The magnetic properties of the system are determined by the competition between Kondo screening and RKKY magnetic exchange. For small values of U/V^2, the Kondo screening dominates and the ground state is a paramagnetic insulator. For large U/V^2, the magnetic exchange dominates, and the system displays an antifer-

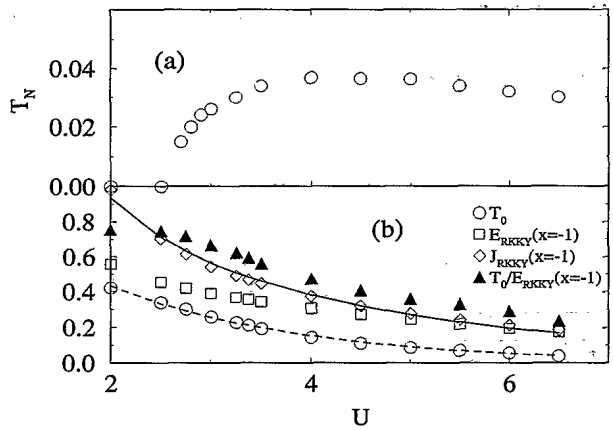

FIG. 11. T_N versus U when $V=0.6$ (a). T_N was determined by extrapolation as shown in Fig. 10. For small U, the system is dominated by Kondo screening, and the ground state is paramagnetic. For large U, the system is dominated by RKKY magnetic exchange, and exhibits an antiferromagnetic transition; however, T_N falls slowly with increasing U. In (b), various relevant energies are plotted versus U when $V=0.6$ and $\beta=10$. T_0 was determined by fitting $\chi_{\text{imp}}(T=0.1)$ to the data shown in Fig. 5. It falls exponentially fast [a fit to an exponential $T_0 = a \exp(-bU)$, is indicated by the dashed line]. The net antiferromagnetic RKKY exchange $J_{\text{RKKY}}(x=-1)$ may be fit to the form $J_{\text{RKKY}}(x=-1) = a + b/U$ as indicated by the solid line. The ratio $T_0/E_{\text{RKKY}}(x=-1)$ falls monotonically with increasing U, indicating that the Kondo screening declines more quickly than the net antiferromagnetic exchange.

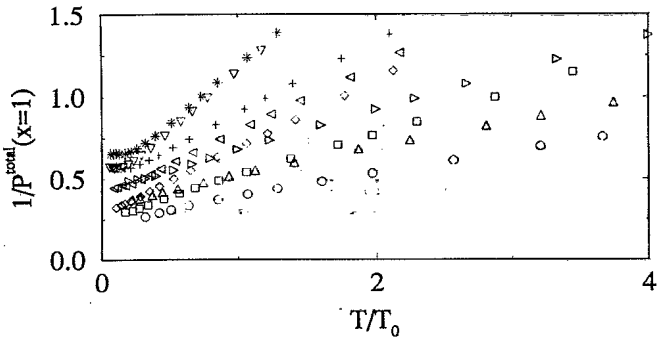

FIG. 12. Inverse odd-frequency pair-field susceptibility vs T. Near a transition the infinite-dimensional limit, $1/P^{\text{total}} \sim (T-T_c)$. In each case, the T_c which would be obtained from the extrapolation $1/P^{\text{total}} \to 0$ would be negative, indicating the lack of a transition.

romagnetic transition. However, the screening still reduces $T_N < E_{\text{RKKY}}(x=-1)$. Furthermore, the fact that the screening diminishes as U increase, and that $J_{\text{RKKY}}(x=-1)$ falls slowly with increasing U, causes T_N to fall only slowly with increasing U after the peak value has been reached.

ACKNOWLEDGMENTS

We would like to acknowledge useful conversations with D. L. Cox, J. Freericks, R. Fye, B. Goodman, J. E. Gubernatis, D. Hess, M. Hundley, R. M. Martin, Th. Pruschke, Matthew Steiner, and F. C. Zhang. This work was supported by the National Science Foundation Grant No. DMR-9107563, the NSF NYI program, and by the Ohio Supercomputing Center.

APPENDIX A: ANALYTIC FORMS OF THE ONE- AND TWO-PARTICLE PROPAGATORS

In the approach discussed in this paper, QMC is used only to extract the irreducible self-energy and local vertex functions. In order to study the properties of the lattice, it is necessary to have analytic forms for the lattice propagators in terms of these functions.

The one-particle propagators can be written as functions of $\Sigma(i\omega_n)$ and complex error function $w(x)$.[16] For example, the one-particle d-band Green's function,

$$G^d(\mathbf{k},i\omega_n)=\frac{1}{i\omega_n-\epsilon_d-\epsilon_{\mathbf{k}}-V^2/[i\omega_n-\epsilon_f-\Sigma(i\omega_n)]}=\frac{1}{\gamma_n-\epsilon_{\mathbf{k}}}\,, \tag{A1}$$

$$G^d(\mathbf{R}=0,i\omega_n)=\frac{1}{N}\sum_{\mathbf{k}}\frac{1}{\gamma_n-\epsilon_{\mathbf{k}}}=\int d\epsilon\,\rho_0(\epsilon)\frac{1}{\gamma_n-\epsilon}=-i\sqrt{\pi}w(\gamma_n)\,, \tag{A2}$$

where $\gamma_n=i\omega_n-\epsilon_d-V^2/[i\omega_n-\epsilon_f-\Sigma(i\omega_n)]$. The f-electron and mixed f-d propagator may be defined in a similar fashion

$$G^f(\mathbf{k},i\omega_n)=\frac{1}{i\omega_n-\epsilon_f-\Sigma(i\omega_n)-V^2/(i\omega_n-\epsilon_d-\epsilon_{\mathbf{k}})}=\frac{\beta_n-\epsilon_{\mathbf{k}}}{\alpha_n(\gamma_n-\epsilon_{\mathbf{k}})}\,, \tag{A3}$$

$$G^f(\mathbf{R}=0,i\omega_n)=[1-i\sqrt{\pi}w(\gamma_n)V^2/\alpha_n]/\alpha_n \tag{A4}$$

$$G^{fd}(\mathbf{k},i\omega_n)=\frac{V}{[i\omega_n-\epsilon_f-\Sigma(i\omega_n)](i\omega_n-\epsilon_d-\epsilon_{\mathbf{k}})-V^2}=\frac{V}{\alpha_n(\gamma_n-\epsilon_{\mathbf{k}})}\,, \tag{A5}$$

$$G^{fd}(\mathbf{R}=0,i\omega_n)=-i\sqrt{\pi}w(\gamma_n)V/\alpha_n\,, \tag{A6}$$

where $\alpha_n=i\omega_n-\epsilon_f-\Sigma(i\omega_n)$ and $\beta_n=i\omega_n-\epsilon_d$.

The two-particle propagators require a bit more thought. However, they may also be written as functions of the appropriate local vertex function and the irreducible self-energy. Consider the local and lattice opposite-spin particle-hole propagators depicted in Fig. 13. Both satisfy a similar two-particle Dyson equation with an identical vertex function $\Gamma(i\omega_n,i\omega_m)$. In fact, if we identify the matrices with elements $\chi^f(\mathbf{q},i\omega_n,i\omega_m)$ and $\chi^f(\mathbf{R}=0,i\omega_n,i\omega_m)$, as $\chi^f_{\mathbf{q}}$ and χ^f_i, respectively, then they satisfy similar matrix equations,

$$\chi^f_{\mathbf{q}}=\chi^{f0}_{\mathbf{q}}+\chi^{f0}_{\mathbf{q}}\Gamma\chi^f_{\mathbf{q}}\,,\quad \chi^f_i=\chi^{f0}_i+\chi^{f0}_i\Gamma\chi^f_i\,, \tag{A7}$$

which may be solved to eliminate the local irreducible vertex function Γ,

$$\chi^{f\,-1}_{\mathbf{q}}=\chi^{f0\,-1}_{\mathbf{q}}+\chi^{f\,-1}_i-\chi^{f0\,-1}_i\,. \tag{A8}$$

Thus, if we measure χ^f_i in the QMC process, and can form χ^{f0}_i and $\chi^{f0}_{\mathbf{q}}$ from $\Sigma(i\omega_n)$, then we can find $\chi^f_{\mathbf{q}}$, and the corresponding magnetic susceptibility,

$$\chi^f(\mathbf{q},T)=2T\sum_{n,m}\chi^f(\mathbf{q},i\omega_n,i\omega_m)\,. \tag{A9}$$

Where the factor of 2 in an isotropic system is required to convert the transverse susceptibility to the more traditional longitudinal value (i.e., $2\chi^{\pm}=\chi^{zz}$).[40]

In fact, since all of the vertex functions are momentum independent or local, the charge and pair-field susceptibilities can be formed by solving a similar set of equations. Finally, we can use the fact that the d electrons are

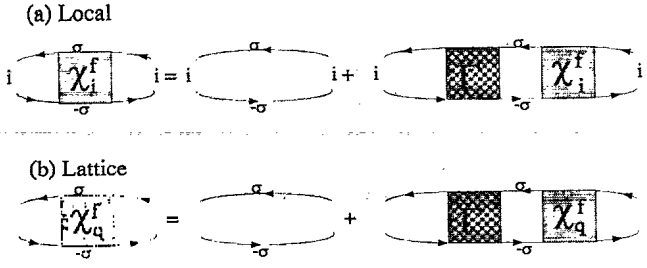

FIG. 13. Two-particle Dyson equations for the local (a) and lattice (b) opposite-spin particle-hole propagators.

noninteracting, so that the vertex function dresses only the f propagators, to form the other lattice propagators. For example, the total lattice particle-hole opposite-spin two-particle propagator is given by

$$\chi_{\mathbf{q}}^{\text{total}}=\chi_{\mathbf{q}}^{d0}-\chi_{\mathbf{q}}^{df0}\chi_{\mathbf{q}}^{fd0}+(\mathbf{I}+\chi_{\mathbf{q}}^{df0}\chi_{\mathbf{q}}^{f0-1}) \times\chi_{q}^{f}(\mathbf{I}+\chi_{\mathbf{q}}^{f0-1}\chi_{q}^{fd0}) . \quad \text{(A10)}$$

The charge and pair-field susceptibilities can be formed by solving a similar set of equations.

Since the local fully dressed magnetic, charge, and pair-field susceptibility matrices are measured in the QMC process, all that we need to calculate the corresponding lattice susceptibilities are the noninteracting results. These may be calculated for any $\mathbf{q}$ by using the methods introduced by Müller-Hartmann[5] who showed that all points $\mathbf{Q}$ in the infinite-dimensional Brillouin zone with the same $x(\mathbf{q})=(1/D)\Sigma_l \cos(q_l)$ are equivalent in that the two-particle density of states may be written as a function of $x(\mathbf{q})$,

$$\rho(\epsilon_1,\epsilon_2)=\frac{1}{N}\sum_{\mathbf{k}}\delta(\epsilon_1-\epsilon_{\mathbf{k}+\mathbf{q}})\delta(\epsilon_2-\epsilon_{\mathbf{k}}) \quad \text{(A11)}$$

$$=\frac{1}{\pi\sqrt{1-x(\mathbf{q})^2}}e^{[\epsilon_1-\epsilon_2 x(\mathbf{q})]^2/[1-x(\mathbf{q})^2]e^{-\epsilon_2^2}} . \quad \text{(A12)}$$

At the zone center $x=1$ and corner $x=-1$, this reduces to

$$\lim_{x\to 1}\rho(\epsilon_1,\epsilon_2)=\frac{1}{\sqrt{\pi}}e^{-\epsilon_1^2}\delta(\epsilon_1-\epsilon_2) , \quad \text{(A13)}$$

$$\lim_{x\to -1}\rho(\epsilon_1,\epsilon_2)=\frac{1}{\sqrt{\pi}}e^{-\epsilon_1^2}\delta(\epsilon_1+\epsilon_2) . \quad \text{(A14)}$$

Using this two-particle density of states, it is possible to find forms for the noninteracting susceptibilities discussed above. For example, the noninteracting particle-hole f-propagator needed to calculate the magnetic and charge susceptibilities is

$$\chi_{\text{ph}}^{f0}(\mathbf{q},i\omega_m)=-\frac{1}{\alpha_n^2}\int d\epsilon_2\rho_0(\epsilon_2)\left[1-\frac{i\sqrt{\pi}V^2 w\{[\gamma_n-\epsilon x(\mathbf{q})]/\sqrt{1-x(\mathbf{q})^2}\}}{\alpha_n\sqrt{1-x(\mathbf{q})^2}}\right]\frac{\beta_n-\epsilon_2}{\gamma_n-\epsilon_2} , \quad \text{(A15)}$$

the corresponding d propagator is

$$\chi_{\text{ph}}^{d0}(\mathbf{q},i\omega_m)=-\int d\epsilon_2\rho_0(\epsilon_2)\frac{-i\sqrt{\pi}w\{[\gamma_n-\epsilon x(\mathbf{q})]/\sqrt{1-x(\mathbf{q})^2}\}}{\sqrt{1-x(\mathbf{q})^2}}\frac{1}{\gamma_n-\epsilon_2} , \quad \text{(A16)}$$

while the mixed propagator is given by

$$\chi_{\text{ph}}^{df0}(\mathbf{q},i\omega_m)=\frac{V^2}{\alpha_n^2}\chi_{\text{ph}}^{d0}(\mathbf{q},i\omega_m) . \quad \text{(A17)}$$

The noninteracting particle-particle f propagator needed to calculate the superconducting susceptibility is

$$\chi_{\text{pp}}^{f0}(\mathbf{q},i\omega_m)=-\frac{1}{|\alpha_n|^2}\int d\epsilon_2\rho_0(\epsilon_2)\left[1-\frac{i\sqrt{\pi}V^2 w[(\gamma_n-\epsilon x(\mathbf{q})]/\sqrt{1-x(\mathbf{q})^2}}{\alpha_n\sqrt{1-x(\mathbf{q})^2}}\right]\frac{\beta_n^*-\epsilon_2}{\gamma_n^*-\epsilon_2} , \quad \text{(A18)}$$

the corresponding d propagator is

$$\chi_{\text{pp}}^{d0}(\mathbf{q},i\omega_m)=-\int d\epsilon_2\rho_0(\epsilon_2)\frac{-i\sqrt{\pi}w\{[\gamma_n-\epsilon x(\mathbf{q})]/\sqrt{1-x(\mathbf{q})^2}\}}{\sqrt{1-x(\mathbf{q})^2}}\frac{1}{\gamma_n^*-\epsilon_2} , \quad \text{(A19)}$$

while the mixed propagator is given by

$$\chi_{\text{pp}}^{df0}(\mathbf{q},i\omega_m)=\frac{V^2}{|\alpha_n|^2}\chi_{\text{pp}}^{d0}(\mathbf{q},i\omega_m) . \quad \text{(A20)}$$

Finally, before leaving this section, we will discuss the formalism necessary to calculate the odd-[39] and even-frequency s-wave pair susceptibility. To do this, we first calculate the particle-particle opposite-spin susceptibility matrix as described above. Then, to project out the odd and even parts, we introduce a frequency form factor $f(i\omega_n)$, so that

$$P=T\sum_{nm}f(i\omega_n)\chi^{\text{total}}(\mathbf{q},i\omega_n,i\omega_m)f(i\omega_m) , \quad \text{(A21)}$$

where, for even-frequency pairing $f(i\omega_n)=1$, and for odd-frequency pairing, $f(i\omega_n)=\text{sgn}(\omega_n)$. Several other odd functions tried for the odd-frequency form factor; however, they did not cause a qualitative change in the results (we never found a pair-field transition).

APPENDIX B: THE RKKY EXCHANGE

The magnetic interaction between the f sites is mediated by two basic types of processes, superexchange and RKKY exchange. Examples of these exchange processes are depicted in Fig. 14 between two f sites. Since there is no direct f-f hybridization, the superexchange is mediated by charge transfer from the f sites to the d band. Both f-electrons first hybridize to the d band, and then hybridize back into the opposite f site. For larger U, $J_{\text{superexchange}} \sim V^4/U^3$. The RKKY process is accomplished by one of the f electrons creating a particle-hole spin excitation in the d band which is absorbed by the other f site. For large U, $J_{\text{RKKY}} \sim J_{fd}^2$ times the d-electron particle-hole bubble. Since the hybridization gap closes as U increases, this bubble should increase with increasing U (in fact, we find that for intermediate to large values of U, it grows roughly linearly with U). So at worst $J_{\text{RKKY}} \sim V^4/U^2$. Thus, for large U, $J_{\text{RKKY}} \gg J_{\text{superexchange}}$. Because of this, and since the magnetic exchange is being calculated only to provide a qualitative result, we will ignore the superexchange.

The RKKY exchange is usually approximated by the second-order (in J_{fd}) process between two f sites, mediated by a particle-hole excitation of the d electrons. If the two f sites are located at $\mathbf{R}$ and $\mathbf{R}'$, with moments $\mathbf{S}_{\mathbf{R}}$ and $\mathbf{S}_{\mathbf{R}'}$ respectively, then the energy of the RKKY exchange process is approximately

$$E_{\text{RKKY}} = -J_{\text{RKKY}} \mathbf{S}_{\mathbf{R}} \cdot \mathbf{S}_{\mathbf{R}'}$$
$$\approx 2J_{fd}^2 T \mathbf{S}_{\mathbf{R}} \cdot \mathbf{S}_{\mathbf{R}'} \frac{1}{N^2} \sum_{\mathbf{k},\mathbf{k}',n} e^{-i\mathbf{k}\cdot(\mathbf{R}-\mathbf{R}')} e^{i\mathbf{k}'\cdot(\mathbf{R}-\mathbf{R}')} \times G^d(\mathbf{k}, i\omega_n) G^d(\mathbf{k}', i\omega_n) , \tag{B1}$$

so that

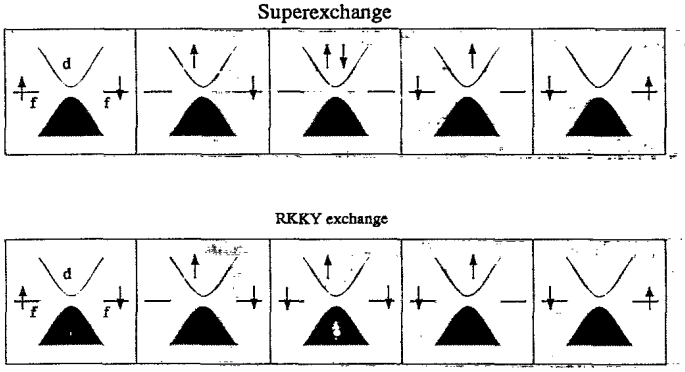

FIG. 14. Examples of the basic electronic processes which characterize the RKKY exchange and superexchange. The top figure illustrates one possible superexchange process. Another process, which is equivalent in the symmetric model, involves double occupancy of one of the f sites. The bottom figure illustrates one of the RKKY processes, which are characterized by particle-hole excitations.

$$J_{\text{RKKY}}(\mathbf{R}-\mathbf{R}') \approx -2J_{fd}^2 T \frac{1}{N^2} \sum_{\mathbf{k},\mathbf{k}',n} e^{-i\mathbf{k}\cdot(\mathbf{R}-\mathbf{R}')} e^{-i\mathbf{k}\cdot(\mathbf{R}-\mathbf{R}')} \times G^d(\mathbf{k}, i\omega_n) G^d(\mathbf{k}', i\omega_n) , \tag{B2}$$

where $J_{fd} \approx 8V^2/U$ in the symmetric model. Then, using the methods discussed in Appendix A, one may calculate the net RKKY exchange between any site and its near-neighbor shell (since there are an infinite number of near neighbors, the exchange between any two sites is zero, but the net exchange is finite),

$$2D\, J_{\text{RKKY}}(\mathbf{R}_{\text{nn}}) = -4J_{fd}^2 T \sum_n [i\sqrt{\pi} w(\gamma_n)\gamma_n + 1]^2 , \tag{B3}$$

and the net exchange between the site and its next-near-neighbor shell,

$$2D(D-1) J_{\text{RKKY}}(\mathbf{R}_{\text{nnn}}) = -J_{fd}^2 T \sum_n [2\gamma_n - i\sqrt{\pi} w(\gamma_n)(1-2\gamma_n^2)]^2 , \tag{B4}$$

where $2D$ and $2D(D-1) \approx 2D^2$ are the number of nearest and next-nearest neighbors, respectively, to each site. In order to determine the net effect of the RKKY exchange, it is also useful to calculate it as a function of $\mathbf{q}$, or rather $x(\mathbf{q})$,

$$J_{\text{RKKY}}(\mathbf{q}) \approx -2J_{fd}^2 T \frac{1}{N} \sum_{\mathbf{k},n} G^d(\mathbf{k}, i\omega_n) G^d(\mathbf{k}+\mathbf{q}, i\omega_n) . \tag{B5}$$

This may be calculated with the formalism discussed in Appendix A for any $x(\mathbf{q})$

$$J_{\text{RKKY}}(x) \approx -2J_{fd}^2 T \sum_n \int d\epsilon \rho_0(\epsilon) \times \frac{1}{\gamma_n - \epsilon} \frac{i\sqrt{\pi} w[(\gamma_n - \epsilon x)/\sqrt{1-x^2}]}{\sqrt{1-x^2}} \tag{B6}$$

We can see from the form of (B3) and (B4) that for the symmetric model, for which γ_n is purely imaginary, the near-neighbor RKKY exchange is antiferromagnetic and the next-near-neighbor exchange is ferromagnetic. Both favor commensurate antiferromagnetism. In fact, the integrated result at different ordering vectors $\mathbf{q}$, $J_{\text{RKKY}}(x(\mathbf{q}))$ displays a peak at $x(\mathbf{q}) = -1$, so that the RKKY exchange favors commensurate antiferromagnetic order.

APPENDIX C: THE IMPURITY KONDO SCALE

Since it is possible to envision the infinite-dimensional PAM as equivalent to a self-consistently embedded Anderson impurity which hybridizes with its (self-consistently determined) host with a matrix element V, it must also be possible to define an impurity Kondo scale T_0.

However, to be consistent with definition of the Kondo scale described by Krishna-murthy, Wilkins, and Wilson[30] one must define the impurity susceptibility as all of

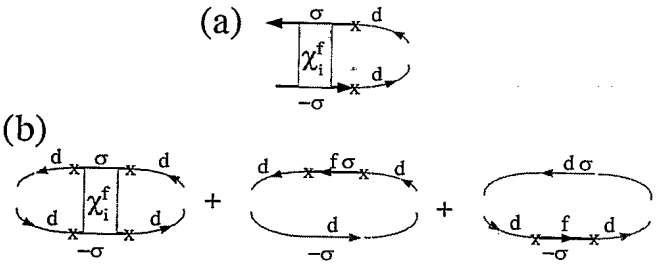

FIG. 15. Diagrams for the (a) $\chi^{fd}_{\rm imp}$ and (b) $\chi^{dd}-\chi^{dd}_{\rm pure\ host}$ contributions to the impurity susceptibility.

the additional magnetic susceptibility due to the addition of the impurity and its subsequent screening by the host:

$$\chi_{\rm imp}=\chi^{ff}_{\rm imp}+\chi^{fd}_{\rm imp}+\chi^{df}_{\rm imp}+\chi^{dd}-\chi^{dd}_{\rm pure\ host}\ , \tag{C1}$$

where $\chi^{ff}_{\rm imp}$ is the f-electron contribution to the impurity susceptibility, $\chi^{fd}_{\rm imp}=\chi^{df}_{\rm imp}$ is the susceptibility involving correlations between the impurity and the host, and $\chi^{dd}-\chi^{dd}_{\rm pure\ host}$ is the additional susceptibility of the host due the introduction of the impurity. Then $T_0=\lim_{T\to 0}1/\chi_{\rm imp}(T)$.

If we assume that the host is described by the fully dressed d-electron propagator obtained once the QMC process has converged, then each of the contributions to $\chi_{\rm imp}$ may be easily calculated. $\chi^{ff}_{\rm imp}$ is local, and hence may easily be calculated in the final iteration of the QMC procedure. The other contributions may be calculated with the knowledge of the host propagator, and the impurity one- and two-particle Green's function. For example, $\chi^{fd}_{\rm imp}$ may be formed by summing the diagrams shown in Fig. 15(a),

$$\chi^{fd}_{\rm imp}=\chi^{df}_{\rm imp}=2TV^2\frac{1}{N}\sum_{\mathbf{k},n,m}\chi^f(i\omega_n,i\omega_m)[G^d(\mathbf{k},i\omega_m)]^2\ . \tag{C2}$$

The momentum sum may be evaluated using the methods described in Appendix A, with the result that

$$\chi^{fd}_{\rm imp}=\chi^{df}_{\rm imp}=-4TV^2\sum_{n,m}\chi^f(i\omega_n,i\omega_m)[i\sqrt{\pi}w(\gamma_n)\gamma_n+1]\ . \tag{C3}$$

Similarly, $\chi^{dd}-\chi^{dd}_{\rm pure\ host}$ may be formed by summing the diagrams shown in Fig. 15(b),

$$\chi^{dd}-\chi^{dd}_{\rm pure\ host}=-4TV^2 2\frac{1}{N}\sum_{\mathbf{q},n}[G^d(\mathbf{q},i\omega_n)]^3G^f(i\omega_n)+2TV^4\frac{1}{N^2}\sum_{\mathbf{q},\mathbf{k},n,m}[G^d(\mathbf{q},i\omega_n)]^2\chi^f(i\omega_n,i\omega_m)[G^d(\mathbf{k},i\omega_m)]^2\ , \tag{C4}$$

or, after the momentum sums are performed

$$\chi^{dd}-\chi^{dd}_{\rm pure\ host}=-4TV^2\sum_n[i\sqrt{\pi}w(\gamma_n)(1-2\gamma_n)-2\gamma_n]G^f(i\omega_n)$$
$$+8TV^4\sum_{n,n}[i\sqrt{\pi}w(\gamma_n)\gamma_n+1]\chi^f(i\omega_n,i\omega_m)[i\sqrt{\pi}w(\gamma_m)\gamma_m+1]\ . \tag{C5}$$

[1]For a recent review, see, N. Grewe and F. Steglich, in *Reports on Physics and Chemistry of Rare Earths,* edited by K. A. Gschneidner, Jr. and L. Eyring (North-Holland, Amsterdam, 1991), Vol. 14, p. 343.

[2]P. Schlottmann, Phys. Rep. **181**, 1 (1989).

[3]D. L. Cox and N. Grewe, Z. Phys. B **71**, 321 (1988).

[4]W. Metzner and D. Vollhardt, Phys. Rev. Lett. **62**, 324 (1989).

[5]E. Müller-Hartmann, Z. Phys. B **74**, 507 (1989); **76**, 211 (1989).

[6]U. Brandt and Ch. Mielsch, Z. Phys. B **75**, 365 (1989); **79**, 295 (1990).

[7]F. J. Ohkawa, Prog. Theor. Phys. Suppl. **106**, 95 (1991).

[8]V. Janiš, Z. Phys. B **83**, 227 (1991); V. Janiš and D. Vollhardt, Int. J. Mod. Phys. B **6**, 731 (1992).

[9]A. Georges and G. Kotliar, Phys. Rev. B **45**, 6479 (1992).

[10]M. Jarrell, Phys. Rev. Lett. **69**, 168 (1992); Th. Pruschke, D. L. Cox, and M. Jarrell, Phys. Rev. B **47**, 3553 (1993); M. Jarrell and Th. Pruschke, Z. Phys. B **90**, 187 (1993).

[11]M. Rosenberg, X. Zhang, and G Kotliar, Phys. Rev. Lett. **69**, 1236 (1992); A. Georges and W. Krauth, *ibid.* **69**, 1240 (1992).

[12]J. E. Hirsch and R. M. Fye, Phys. Rev. Lett. **56**, 2521 (1986).

[13]A. Georges, G. Kotliar, and Q. Si, Int. J. Mod. Phys. B **6**, 705 (1992).

[14]M. Jarrell, H. Akhlaghpour, and Thomas Pruschke, in *Quantum Monte Carlo Methods in Condensed Matter Physics,* edited by M. Suzuki (World Scientific, Singapore, 1993).

[15]R. K. Bryan, Euro. Biophys. J. **18**, 165 (1990); J. E. Gubernatis *et al.*, Phys. Rev. B **44**, 6011 (1991); R. N. Silver *et al.*, *ibid.* **41**, 2380 (1989).

[16]*Handbook of Mathematical Functions,* edited by M. Abramowitz and I. E. Stegun (Dover, New York, 1972), p. 297.

[17]A. Khurana, Phys. Rev. Lett. **64**, 1990 (1990).

[18]G. Czycholl and H. J. Leder, Z. Phys. B **44**, 59 (1981); D. L. Cox, C. Tannous, and J. W. Wilkins, Phys. Rev. B **33**, 2132 (1986).

[19]T. Takabatake *et al.*, Phys. Rev. B **41**, 9607 (1990).

[20]M. F. Hundley *et al.*, Phys. Rev. B **42**, 6842 (1990).

[21]A. Severing *et al.*, Phys. Rev. B **44**, 6832 (1991).

[22]K. Yamada and K. Yoshida, in *Theory of Heavy Fermions and Valence Fluctuations,* edited by T. Kasuya and T. Saso, Springer Series in Solid State Sciences Vol. 62 (Springer, New York, 1985).

[23]Th. Pruschke and N. Grewe, Z. Phys. B **74**, 439 (1989).

[24]N. Grewe, Solid State Commun. **50**, 19 (1984).

[25]The size of the gap depends upon the way it is measured. For example, if the gap is measured from $\omega=0$ to the position of half the maximum height, then its width is roughly $\Delta \approx T_0/3$.
[26]R. M. Fye and D. J. Scalapino, Phys. Rev. Lett. **65**, 3177 (1990).
[27]C. C. Yu and S. R. White, Phys. Rev. Lett. **71**, 3866 (1993).
[28]K. G. Wilson, Rev. Mod. Phys. **47**, 773 (1975).
[29]When $\langle (n_{f\sigma}-n_{f-\sigma})^2 \rangle$ is small (cf. Fig. 8), $1/T_0\chi_{\rm imp}(T)$ vs T/T_0 shows deviations from scaling when $T/T_0 > 1$. This is expected when the model is less correlated.
[30]H. R. Krishna-murthy, J. W. Wilkins, and K. G. Wilson, Phys. Rev. B **21**, 1003 (1979)
[31]V. Zlatić and B. Horvatić, Phys. Rev. B **28**, 6904 (1988).
[32]T. M. Rice and K. Ueda, Phys. Rev. B **34**, 6420 (1986).
[33]T. Saso and Y. Seino, J. Phys. Soc. Jpn. **55**, 3729 (1986).
[34]R. M. Fye, Phys. Rev. B **41**, 2490 (1990).
[35]S. Yip, Phys. Rev. B **38**, 8785 (1988).
[36]S. Doniach, Physica (Utrecht) **91B**, 231 (1977); in *Valence Instabilities and Related Narrow-Band Phenomena,* edited by R. D. Park (Plenum, New York, 1977).
[37]S.-J. Sun, M.-F. Yang, and T.-M. Hong, Phys. Rev. B **48**, 16 127 (1993).
[38]P. Coleman, E. Miranda, and A. Tsvelik, Phys. Rev. Lett. **70**, 2960 (1993).
[39]V. L. Berezinski, Pis'ma Zh. Eksp. Teor. Fiz. **20**, 628 (1974) [JETP Lett. **20**, 287 (1974)].
[40]See, for example, S. Doniach and E. H. Sondheimer, *Green's Functions for Solid State Physicists,* edited by David Pines, Frontiers in Physics Lecture Note and Reprint Series No. 44 (Benjamin/Cummings, London, 1974).